Office of Naval Research

Contract Nonr 1866(02)

Technical Report No.5

BUCKLING OF CLAMPED SHALLOW SPHERICAL SHELLS

By

Bernard Budiansky

Division of Engineering and Applied Physics
Harvard University
Cambridge, Massachusetts

August 1959

OFFICE OF NAVAL RESEARCH

Contract Nonr 1866(02)

Technical Report No. 5

BUCKLING OF CLAMPED SHALLOW SPHERICAL SHELLS

by

Bernard Budiansky

Division of Engineering and Applied Physics
Harvard University
Cambridge, Mass.

August 1959

BUCKLING OF CLAMPED SHALLOW SPHERICAL SHELLS[1]

by

Bernard Budiansky

1. INTRODUCTION

This paper is concerned with the axisymmetric buckling under uniform pressure of a shallow portion of a spherical shell, clamped along a circular boundary (Fig. 1). The same problem has been the subject of several previous theoretical investigations (Refs. 1-7). Although these previous studies were all based on the same non-linear differential equations, the results found, by a variety of techniques, are generally in disagreement with each other. Some of the trouble in these solutions is evidently related to the waviness of the shell distortions, which tends to increase with decreasing shell thickness. The present analysis, which exploits an integral-equation formulation of the problem, should give results of uniform accuracy for all thicknesses.

Some qualitative information concerning the buckling of complete spherical shells may be recalled. According to the classical theory, a complete, initially perfect spherical shell subjected to external pressure contracts in size, without bending, until the buckling pressure q_o is reached; after buckling (Ref. 8), the pressure needed for equilibrium drops sharply (see curve A, Fig. 2). On the other hand, initial geometrical imperfections in the complete spherical shell permit bending to start immediately upon the application of pressure, and the subsequent

---

[1] For presentation at the IUTAM Symposium on the Theory of Thin Elastic Shells, Delft, Netherlands, August 1959. This work was sponsored by the Office of Naval Research under Contract Nonr 1866(02) with Harvard University.

non-linear variation of pressure with deflection leads to a local maximum q_{cr} of the pressure (see curves B, C, Fig. 2), at which point buckling - or snapping - occurs. Experiments show that buckling pressures of complete spherical shells are substantially lower than q_o, and it is now generally believed that initial imperfections are responsible for this disagreement.

In contrast to the behavior of the perfect complete sphere, the perfect clamped shallow shell distorts axisymmetrically out of the spherical shape at the beginning of loading; in effect, the pressure makes its own "initial" imperfections, and so, as in the case of the imperfect complete sphere, buckling of the perfect clamped shell may be related to the local maximum q_{cr} of the pressure as bending proceeds. It does not necessarily follow, however, that initial geometrical imperfections in the shallow shell may be disregarded. In fact, for sufficiently small shell thickness, the early bending deformation of a perfect shallow spherical shell under uniform pressure is confined to a narrow "boundary layer" near the edge, with the rest of the shell remaining essentially spherical (Ref. 9). Consequently, as thickness decreases, q_{cr} of the initially perfect shallow shell is expected to approach q_o of the corresponding complete sphere, and experimental confirmation would then not be anticipated unless geometrical imperfections were taken into account.

In the present paper, results are found for the axisymmetric buckling pressures of perfect clamped shells, as well as of shells having small axisymmetric initial geometric imperfections. (Similar imperfections were also considered in Ref. 7). It should be noted, however, that axisymmetric buckling does not necessarily correspond to the lowest buckling pressure of the initially perfect shell; the possibility exists

that an instability associated with unsymmetrical distortions may occur before the axisymmetric buckling pressure is reached. Furthermore, unsymmetrical initial imperfections might have a more significant effect than axisymmetric ones; although this conjecture is not explored analytically in this paper, some qualitative observations concerning its likelihood are made.

2. BASIC EQUATIONS

The basic relations of non-linear shallow shell theory (Ref. 10) will be reproduced for the case of axisymmetric deformations of shells of revolution subjected to uniform pressure.

Moment equilibrium (see Figs. 1 and 3) requires

$$\frac{d}{dr}(rM_r) - M_t - rQ = 0 \tag{1}$$

horizontal force equilibrium gives

$$\frac{d}{dr}(rN_r) - N_t = 0 \tag{2}$$

and vertical equilibrium of a polar cap gives

$$rQ + \frac{qr^2}{2} + rN_r\left(\frac{dw}{dr} - \frac{dz_o}{dr}\right) = 0 \tag{3}$$

where M_r, M_t, N_r, N_t and Q are moments and forces per unit length as shown in Fig. 3, q is the pressure, w is the vertical downward displacement, and z_o defines the shell middle surface, as shown in Fig. 1.

The generalized force-distortion relations are

$$\frac{du}{dr} - \frac{dz_o}{dr}\frac{dw}{dr} + \frac{1}{2}\left(\frac{dw}{dr}\right)^2 = \frac{1}{Et}(N_r - \nu N_t) \tag{4}$$

$$\frac{u}{r} = \frac{1}{Et}(N_t - \nu N_r) \tag{5}$$

$$\frac{d^2w}{dr^2} = -\frac{12}{Et^3}(M_r - \nu M_t) \tag{6}$$

$$\frac{1}{r}\frac{dw}{dr} = -\frac{12}{Et^3}(M_t - \nu M_r) \tag{7}$$

where u is the horizontal displacement, t is the shell thickness, E is Young's modulus, and ν is Poisson's ratio.

Relating the membrane forces N_r and N_t to a stress function ψ by

$$N_r = \frac{\psi}{r} \tag{8}$$

and

$$N_t = \frac{d\psi}{dr} \tag{9}$$

provides satisfaction of (2); eliminating M_r, M_t and Q from (1), (3), (6), and (7) gives

$$\frac{Et^3}{12(1-\nu^2)}\left\{\frac{d}{dr}\left(r\frac{d\beta}{dr}\right) - \frac{\beta}{r}\right\} - \left(\frac{dz_o}{dr}\right)\psi = -qr^2 + \psi\beta \tag{10}$$

where $\beta = -\frac{dw}{dr}$ is the rotation of an element of the shell (see Fig. 3). Finally, elimination of the displacement u from (4) and (5) provides the compatibility equation

$$\frac{1}{Et}\left\{\frac{d}{dr}\left(r\frac{d\psi}{dr}\right) - \frac{\psi}{r}\right\} + \left(\frac{dz_o}{dr}\right)\beta = -\frac{1}{2}\beta^2 \tag{11}$$

The simultaneous equations (10) and (11) for the variables β and ψ are equivalent to the equations governing the analyses of Refs. 1-7.

The boundary conditions appropriate for the clamped shell are

$$\beta = 0 \quad \text{at} \quad r = a \tag{12}$$

and, as a consequence of Eq. (5) and the requirement that u vanish at the edge,

$$\frac{d\psi}{dr} - \nu \frac{\psi}{r} = 0 \quad \text{at} \quad r = a \tag{13}$$

In addition, conditions of finiteness of β and ψ are imposed at $r = 0$.

Within the framework of shallow shell theory, an initial spherical shape is represented by the parabola

$$z_o = H \left[1 - (\frac{r}{a})^2\right] \tag{14}$$

where (see Fig. 1) H is the shell "rise". Then, introduction of the geometrical parameter λ defined by

$$\lambda^4 = 48(1-\nu^2)(\frac{H}{t})^2 \tag{15}$$

and substitution of the non-dimensional variables

$$x = \frac{\lambda r}{a} \tag{16}$$

$$\theta = (\frac{\lambda a}{2H})\beta \tag{17}$$

$$\bar{\phi} = \left[\frac{12(1-\nu^2)a}{\lambda E t^3}\right] \psi \tag{18}$$

into Eqs. (10) and (11) give for the initially perfect spherical shell the non-dimensional equations

$$(x\theta')' - \frac{\theta}{x} + x\bar{\phi} = -2px + \theta\bar{\phi} \tag{19}$$

$$(x\bar{\phi}')' - \frac{\bar{\phi}}{x} - x\theta = -\frac{1}{2}\theta^2 \tag{20}$$

where primes denote differentiation with respect to x. Here the non-dimensional pressure parameter p is defined as

$$p = \frac{q}{q_o} \tag{21}$$

where

$$q_o = \frac{2E}{\sqrt{3(1-\nu^2)}} \left(\frac{t}{R}\right)^2 \tag{22}$$

is the classical buckling pressure of a complete spherical shell having the same radius of curvature $R = \frac{a^2}{2H}$ as the shallow shell under consideration. The boundary conditions (12) and (13) transform to

$$\theta(\lambda) = 0 \tag{23}$$

and

$$\lambda \bar{\phi}'(\lambda) - \nu \bar{\phi}(\lambda) = 0 \tag{24}$$

Note that in the present non-dimensional formulation the geometrical parameter λ determines the interval in the x coordinate in which the differential equations (19) and (20) apply, but does not appear explicitly in these equations.

According to Reissner (Ref. 9) the shallowness requirement is roughly $H/a \leq 1/6$. This restriction is quite independent of the parameter λ, which may be as large as desired. To avoid confusion, it is best to regard H and a as fixed in magnitude, and to think of small λ's as representing thick shells, whereas large λ's correspond to thin shells. The remark in Section 1 concerning the expected variation of buckling pressure with thickness can now be made more precise: as λ becomes infinite, $p_{cr} (= q_{cr}/q_o)$ for the initially perfect shallow shell should approach 1.

The surface of a shallow shell whose initial configuration deviates axisymmetrically from perfect sphericity may be represented by

$$z_o = H\left[1 - \left(\frac{r}{a}\right)^2 - \varepsilon e(r)\right] \tag{25}$$

where $e(r)$ is the shape of the imperfection. In this case, the equations analogous to (19) and (20) become

$$(x\theta')' - \frac{\theta}{x} + x\bar{\phi} = -2px + \theta\bar{\phi} + \varepsilon h\bar{\phi} \tag{26}$$

$$(x\bar{\phi}')' - \frac{\bar{\phi}}{x} - x\theta = -\frac{1}{2}\theta^2 - \varepsilon h\theta \tag{27}$$

where

$$h = -\frac{\lambda^2}{2}\frac{de}{dx} \tag{28}$$

and the boundary conditions (23) and (24) continue to apply. Eqs. (26) and (27) reduce, of course, to (19) and (20) when $\varepsilon = 0$.

In the present study, the shape of the initial imperfection was chosen as

$$e(r) = \left[1 - \left(\frac{r}{a}\right)^2\right]^2 \tag{29}$$

For this choice, ε equals the ratio of the <u>downward</u> initial displacement at the center of the shell to the rise H of the perfect shell.

It should be noted that, in shallow shell theory, an initial parabolic shape does <u>not</u> constitute a deviation from "perfect" sphericity; thus the non-linear differential equations (19) and (20) are satisfied exactly by the membrane state

$$\begin{cases} \theta = 0 \\ \bar{\phi} = -2px \end{cases}$$

This state does not, however, satisfy the fixity condition (24), and so bending of the clamped shell must occur for all p.

3. REVIEW OF PREVIOUS WORK

Figure 4 summarizes the results of previous attempts to calculate p_{cr} of the initially perfect clamped shell. Feodosiev (Ref. 1.) applied the Galerkin method, using simple polynomial functions, to obtain approximate solutions of the governing non-linear equations. Kaplan and Fung (Ref. 2) obtained the first two terms in a power series expansion of p versus $w(0)$; in their procedure, the non-linear differential equations were reduced to a set of linear equations by a perturbation technique. They were able to find results for p_{cr} , as determined by the condition $\frac{dp}{dw(0)} = 0$, only for relatively low values of λ . (Kaplan and Fung also obtained one improved value of p_{cr} for $\lambda = 4$ by solving several more of their perturbation equations -- by finite difference approximations -- to get four terms in the power series for p). Archer (Ref. 3) recognized that for higher values of λ the variation of $w(0)$ with p is not necessarily monotonic, and accordingly used the deflection at some intermediate station, when necessary, in a perturbation expansion similar to that of Kaplan and Fung. Archer solved his linear perturbation equations approximately by means of a finite number of terms in a Fourier-Bessel expansion. Note that Archer's results for p_{cr} do appear to approach 1 as λ increases. Reiss, Greenberg, and Keller (Ref. 4) tried power series solutions of the non-linear differential equations; for a given value of λ , they looked for solutions at successive increments of p , and presumed that p_{cr} had been exceeded when the search proved fruitless. Their results are embodied in the collection of vertical intervals shown in Fig. 4, within each of which p_{cr} is supposed to lie. A very

similar power series technique was utilized independently by Weinitschke (Ref. 5) who obtained definite results for p_{cr} only for $\lambda \leq 5$; but at several higher values of λ (see the dotted curve in Fig. 4), he succeeded in finding solutions to the non-linear equations at values of p above those where Reiss, Greenberg and Keller failed. According to Weinitschke, the values of p along the dotted portion of his curve constitute only lower bounds to the correct values of p_{cr} . Finally, Chen (Ref. 6), improving upon a procedure used by von Willich (Ref. 7), carried out a Rayleigh-Ritz solution on the basis of a variational equation equivalent to the governing non-linear differential equations; Chen used a sixth degree polynomial (with two free parameters) for the representation of the deflection.

The results of the more recent studies of Refs. 3-6 are in fairly good agreement in the narrow range between $\lambda = 4$ and $\lambda = 5$; beyond this range, the results do not encourage confident conclusions concerning the correct theoretical variation of p_{cr} with λ .

4. FORMULATION OF INTEGRAL EQUATIONS

A pair of integral equations equivalent to the differential equations (26) and (27) together with the boundary conditions (23) and (24) will now be constructed. Consider the equations

$$L(y) + xz = r \tag{30}$$

$$L(z) - xy = s \tag{31}$$

where $L(\ )$ is the operator $x(\ )' - \frac{1}{x}(\ )$. Assume that the functions r and s vanish for $x > \lambda$, but seek a solution of (30) and (31) valid for all $x > 0$, and bounded at infinity. Application of the

Hankel transform

$$y^{*}(\alpha) \int_0^{\infty} xJ_1(\alpha x)y(x)dx \qquad (32)$$

to (30) and (31), and use of the relation (Ref. 11)

$$\left[\frac{L(y)}{x}\right]^{*} = -\alpha^2 y^{*}$$

provides the transformed equations

$$-\alpha^2 y^{*} + z^{*} = \left(\frac{r}{x}\right)^{*}$$

$$-\alpha^2 z^{*} - y^{*} = \left(\frac{s}{x}\right)^{*}$$

whence

$$y^{*} = \frac{-\alpha^2\left(\frac{r}{x}\right)^{*} - \left(\frac{s}{x}\right)^{*}}{\alpha^4+1}$$

$$z^{*} = \frac{-\alpha^2\left(\frac{s}{x}\right)^{*} + \left(\frac{r}{x}\right)^{*}}{\alpha^4+1}$$

Then application of the inversion formula

$$y(x) = \int_0^{\infty} \alpha J_1(\alpha x)y^{*}(\alpha)d\alpha$$

and interchange of orders of integration gives

$$y(x) = \int_0^{\lambda} G(x,\xi)r(\xi)d\xi + \int_0^{\lambda} H(x,\xi)s(\xi)d\xi \qquad (33)$$

$$z(x) = -\int_0^{\lambda} H(x,\xi)r(\xi)d\xi + \int_0^{\lambda} G(x,\xi)s(\xi)d\xi \qquad (34)$$

where the symmetrical kernels G and H are

$$G(x,\xi) = -\int_0^\infty \left(\frac{\alpha^3}{\alpha^4+1}\right) J_1(\alpha x)J_1(\alpha\xi)d\xi \qquad (35)$$

$$H(x,\xi) = -\int_0^\infty \left(\frac{\alpha}{\alpha^4+1}\right) J_1(\alpha x)J_1(\alpha\xi)d\xi \qquad (36)$$

These infinite integrals are evaluated in Appendix A, with the results, in terms of Kelvin functions,

$$\begin{aligned} G(x,\xi) &= \text{bei}'x\ \text{ker}'\xi + \text{ber}'x\ \text{kei}'\xi \qquad (0 \le x \le \xi) \\ &= \text{bei}'\xi\ \text{ker}'x + \text{ber}'\xi\ \text{kei}'x \qquad (0 \le \xi \le x) \end{aligned} \qquad (37)$$

and

$$\begin{aligned} H(x,\xi) &= \text{ber}'x\ \text{ker}'\xi - \text{bei}'x\ \text{kei}'\xi \qquad (0 \le x \le \xi) \\ &= \text{ber}'\xi\ \text{ker}'x - \text{bei}'\xi\ \text{kei}'x \qquad (0 \le \xi \le x) \end{aligned} \qquad (38)$$

Next, with a view to the ultimate enforcement of boundary conditions at $x = \lambda$, define the functions $A_1(x)$ and $B_1(x)$ as the solutions of the homogeneous equations

$$L(A) + xB = 0 \qquad (39)$$

$$L(B) - xA = 0 \qquad (40)$$

and the non-homogeneous boundary conditions

$$A_1(\lambda) = 0 \qquad (41)$$

$$\lambda B_1'(\lambda) - \nu B_1(\lambda) = 1 \qquad (42)$$

Similarly, let $A_2(x)$ and $B_2(x)$ be the solutions of (39) and (40) that satisfy

$$A_2(\lambda) = 1 \qquad (43)$$

$$\lambda B_2'(\lambda) - \nu B_2(\lambda) = 0 \qquad (44)$$

Formulas for A_1, A_2, B_1 and B_2 are readily found in terms of Kelvin

functions (see very similar calculations in Ref. 12) and are displayed in Appendix B.

The desired integral equations can now be formulated; it can be verified that a solution θ , $\bar{\phi}$ of the non-linear system (26), (27), (23), and (24) satisfies the equations

$$\theta(x) = y(x) + dA_1(x) + eA_2(x) \tag{45}$$

$$\bar{\phi}(x) = z(x) + dB_1(x) + eA_2(x) - 2px \tag{46}$$

where $y(x)$ and $z(x)$ are given by (33) and (34), with

$$r = \theta\bar{\phi} + \varepsilon h\bar{\phi} \tag{47}$$

$$s = -\frac{1}{2}\theta^2 - \varepsilon h\theta \tag{48}$$

and where

$$e = -y(\lambda) \tag{49}$$

$$d = 2p\lambda(1-\nu) - \left[\lambda z'(\lambda) - \nu z(\lambda)\right] \tag{50}$$

This formulation still contains a single differentiation, in Eq. (50) for the scalar d . But note that, from (31),

$$(x^2z')' - (xz)' - x^2y = xs$$

whence

$$\lambda^2 z'(\lambda) - \lambda z(\lambda) = \int_0^\lambda (x^2y + xs)dx$$

Hence, Eq. (50) may be replaced by

$$d = 2p\lambda(1-\nu) - (1-\nu)z(\lambda) - \frac{1}{\lambda}\int_0^\lambda (x^2y + xs)dx \tag{51}$$

The integral Eqs. (45) and (46) constitute the basis for the present analysis. Two different viewpoints, each corresponding to well defined

physical conditions, may be adopted for the solution of these equations. The pressure parameter p may be regarded as prescribed and monotonically increasing, and solutions for θ and ϕ sought; this specification of the pressure corresponds to loading the shell by pressurized air in a chamber of large volume. Alternately, the average deflection can be specified, and a solution found for p, as well as θ and ϕ; this approach represents pressure loading by a relatively incompressible fluid (say mercury), the volume of which is under control at all times. The average deflection is

$$\bar{w} = \frac{2}{a^2} \int_0^a rw \, dr$$

from which, by integration by parts and use of the conditions $w = dw/dr = 0$ at $r = a$,

$$\bar{w} = \frac{2H}{\lambda^4} \int_0^\lambda x^2 \theta \, dx \tag{52}$$

The convenient average-deflection parameter

$$\rho = \frac{\lambda^2}{2} \frac{\bar{w}}{H} = 2 \left[3(1-\nu^2)\right]^{\frac{1}{2}} \left(\frac{\bar{w}}{t}\right) \tag{53}$$

may be introduced; then

$$\rho = \frac{1}{\lambda^2} \int_0^\lambda x^2 \theta \, dx \tag{54}$$

Figure 5 shows hypothetical curves of p versus ρ for the clamped shallow shell. In case (a), the $p - \rho$ relationship is one-to-one, and no buckling occurs; in cases (b) and (c), a pressure monotonically increasing from zero causes buckling as soon as the first

local maximum of the curve, p_{cr}, is exceeded. On the other hand, if the average deflection were assumed to increase monotonically, there would be no sudden snapping of the shell in case (b), but the pressure would still reach a maximum value p_{cr}, and then decrease smoothly. In case (c), again under prescribed, increasing average deflection, the shell would tend to snap from point (1) -- just after a small reduction of p from p_{cr} -- to point (2), with a sudden drop in pressure. (The designation p_{cr} will be retained for the pressure maximum, even though snapping does not occur at p_{cr} under the prescribed volume type of loading.) The most precise determination of p_{cr} in cases (b) and (c) would be accomplished analytically by letting ρ increase in sufficiently small increments and following the resulting $p - \rho$ curve beyond its first maximum. Alternatively, as was attempted in Ref. 4, close bounds on p_{cr} can be deduced by letting p increase in small increments until, for some increment in p, no "adjacent" equilibrium position is found to exist. Finally, the unlikely-looking hypothetical $p - \rho$ curve shown in Fig. 5 cannot be ruled out on theoretical grounds, but no evidence of its occurrence was found in any of the cases actually calculated. (Note, however, that such curves may be found when the pressure is plotted against the deflection at some particular point in the shell instead of against the <u>average</u> deflection.)

5. ITERATIVE PROCEDURE

With either p or ρ considered prescribed, an iterative procedure for the solution of Eqs. (45) and (46), can now be formulated. If p is prescribed, an initial guess for θ and ϕ may be substituted into the formulas (33) and (34) for $y(x)$ and $z(x)$, next the constants e and d

can be calculated by Eqs. (49) and (51), and then the subsequent approximation to θ and ϕ may be found from Eqs. (45) and (46). The value of ρ corresponding to the new θ and ϕ can be found conveniently by use of the equation

$$\rho = \frac{1}{\lambda^2} \int_0^\lambda x^2 y \, dx + d\rho_1 + e\rho_2 \tag{55}$$

where the constants

$$\rho_1 = \frac{1}{\lambda^2} \int_0^\lambda x^2 A_1(x) dx \tag{56}$$

and

$$\rho_2 = \frac{1}{\lambda^2} \int_0^\lambda x^2 A_2(x) dx \tag{57}$$

are calculated in Appendix B. The entire process may then be repeated, and a point on the $p - \rho$ curve is finally determined when successive values of ρ converge to sufficient accuracy.

If ρ is prescribed, $y(x)$ and $z(x)$ are found in the same way, and so is e, but d is calculated from Eq. (55), and Eq. (51) is then used to solve for the current approximation to p. Again, the process is repeated until, this time, the values of p converge to a limit.

In the application of these procedures, the integrations involved in Eqs. (33), (34), (51) and (54) were performed numerically on the basis of Simpson's rule, and the iterative procedure was formulated in terms of matrix operations. (Special integration formulas were devised for the integrations involving the kernel $G(x,\xi)$, which has discontinuous first

derivatives at $x = 0$.)

The spacing of stations in the numerical integration is very important; in this work the invariant spacing $\Delta x = .25$ was chosen for all λ, leading to matrices of order 4λ. (Since θ and ϕ vanish at $x = 0$, the station at the origin could be omitted in the matrix set-up.) This choice of interval was motivated primarily by consideration of the waviness of the expected deformation at buckling; the higher λ, the more waves are expected, with a roughly constant half-wave-length, in terms of x, of about 3 (see Appendix C). The use of about twelve stations per half-wave-length in Simpson's rule was considered adequate for acceptable accuracy. (It happens, also, that the choice $\Delta x = .25$ provides a reasonable number of stations within the boundary layer of early bending deformation.) The price paid, of course, for uniform accuracy over all values of λ was the necessity of handling matrices of increasingly higher order as λ increased. The use of high-speed electronic computation was essential; an IBM 704 digital computer was used to obtain the numerical results presented in the next section.[†]

6. NUMERICAL RESULTS

The results obtained for the variation of p_{cr} with λ were established by a combination of the two iterative procedures discussed. Fig. 6(a) shows some $p - \rho$ curves for the initially perfect shell obtained by letting ρ be the prescribed variable, and following the curve over the first maximum of p. (Poisson's ratio ν was taken equal to 1/3 in all

---

[†] The author is indebted to Mr. Morris Waters for programming the problem.

calculations.) Points on these curves were found by starting with a relatively low value of ρ, then letting ρ increase in increments of .1, and finally, when necessary, going back to the vicinity of p_{cr} with smaller increments of ρ (.01 - .02) to establish p_{cr} more accurately. In these calculations, the final results for θ and ϕ at a given ρ were used as the initial guesses for θ and ϕ at the next incremented value of ρ. At each ρ, the convergence criterion was that the final answer for p agree to three decimal places with the mean of the results of the five previous iterations.

In some cases (for example, $\lambda = 5.5$, 9, $\varepsilon = 0$, Fig. 6(b)), the peak of the $p - \rho$ curve was evidently so sharp, and the subsequent decrease in ρ as well as p so sudden (see Fig. 5(c)), that increments of .02 in ρ were too large to map the top of the curve. Thus, for $\lambda = 9$, the $p - \rho$ variation was monotonic up to $\rho = 1.34$, but at $\rho = 1.36$ (shown by the vertical bar in Fig. 6(b)) the iterative procedure suddenly failed to converge. The curve was then corroborated by use of the other procedure; p was varied in increments of .01, and at $p = .94$, shown by the horizontal bar in Fig. 6(b), no convergence for ρ was found. The loss of convergence was spectacular; at $p = .93$, ρ converged after 12 iterations, but 105 iterations were insufficient at $p = .94$. The value of p_{cr} for $\lambda = 9$, may therefore be presumed to be less than .94, but certainly greater than .931, the value obtained for $\rho = 1.34$.

For most of the other values of λ (and ε) considered, the procedure based on assigning ρ was omitted altogether, and only p was varied in increments of .01 with the aim of establishing sufficiently close bounds

on p_{cr}. In most cases, the sudden failure to converge to a definite value of ρ at some value of p was as dramatic as for $\lambda = 9$.

The results found for p_{cr} at all the values of λ and ε considered are given in Table 1. Where a single number is given for p_{cr}, the procedure was to assign ρ and pinpoint accurately the top of the $p - \rho$ curve. Where two numbers are shown, the higher value corresponds to an unconverged iteration with p assigned, and the lower number is a definite pre-buckling value of p obtained by prescribing either ρ or p, as indicated in the Table.

The results are shown in Fig. 7 as curves of p_{cr} versus λ, for various values of ε. The crosses on these curves correspond to the cases where the maximum of the $p - \rho$ curves were precisely located; the solid dots show the points for which only bounds on p_{cr} were found, with the diameter of the dots equal to or greater than the interval of uncertainty. Strictly speaking, it must be conceded that the upper bounds in these cases have not been rigorously established, since it is conceivable that failure to converge might be due to some unknown cause other than the non-existence of an adjacent equilibrium position. But the value of p at the base of each dot is definitely a lower bound to the correct value of p_{cr}.

Also shown in Fig. 7 are experimental points obtained by Kaplan and Fung (Ref. 2) and Homewood, Brine and Johnson (Ref. 13). The significance of the present theoretical results and their relation to these experiments will be assessed in the discussion that follows.

7. DISCUSSION OF RESULTS

Comparison of Fig. 7 and Fig. 4 reveals that only for $\lambda \leq 5$ are the

present results for the initially perfect shell ($\varepsilon = 0$) in fairly good agreement with those of Archer, Reiss et al, Weinitschke, and Chen; for λ up to 6, Chen's energy solution remains in fair agreement with the present ones; but for $\lambda > 6$, the present results bear little resemblance to the only other previously available ones of Archer and Reiss et al. In common with the results of Archer, the present values of p_{cr} appear to approach 1 as λ increases, but do so in an oscillatory fashion rather than monotonically as Archer found.

Some explanation for the details of the oscillatory variation of p_{cr} with λ is afforded by the results of a simple analysis of the buckling and post-buckling behavior of a shallow shell having boundary conditions that are slightly different from those of complete edge fixity. This modified shell is shown by the upper sketch in Fig. 8; rotation of the edges is still fully constrained, but motion normal to the surface is freely permitted at the boundary. Thus, just as the complete sphere does, this modified shell contracts without bending under uniform pressure until buckling occurs. The scalloped curve in Fig. 8 shows the results for p_{cr} obtained from an exact solution given in Appendix C; each scallop corresponds to the lowest of the eigenvalues in the spectrum of critical pressures that exists for every λ. (Note that the minimum of each scallop is at $p = 1$.) The post-buckling behavior of the modified shell is also analyzed in Appendix C by means of a simple (but approximate) Galerkin solution; typical results, for four values of λ, are shown in Fig. 9. (At any λ, separate post-buckling curves of p versus ρ emanate from each eigenvalue, and so more than one such curve can often be plotted in the ranges of p and ρ shown.) The index n denotes

the order of the buckling mode shape, and is numerically equal to the number of nodal circles. The shape of these post-buckling curves indicates, of course, that initial imperfections might have an important influence on the buckling pressure of the modified shell. Note, however, that these curves are explicitly based on the assumption that the center buckling deflection is downward; the sign of the eigenfunction of the linear buckling problem is indeterminate, but the assumption of an upward buckle at the center would lead to $p - \rho$ curves that continue to rise sharply after buckling.

The shape of the p_{cr} versus λ curve of the fully clamped shell, shown for comparison in Fig. 8, can now be rationalized. Around $\lambda = 4$, the curve is roughly similar to the first scallop of the modified shell, but substantially lower; this is because the rotations produced by the pressure, having the distribution shown by the top curve in Fig. 10(a), is very similar to the buckling rotations (Fig. 10(b)) of the modified structure. The clamped shell is predisposed to a similar buckling mode, and so the initial rotations produced by the pressure are of just the right kind to trigger buckling. Around $\lambda = 7$, on the other hand, Fig. 10 shows that the early rotations could hardly be less sympathetic to the natural buckling rotations; note that the sign of the buckling rotations, discussed above, is important in this comparison. The result is that buckling is delayed until p reaches values somewhat above 1, the initial distortions being of little or no help in inducing buckling in the preferred second mode shape. (The hesitant, wavering, approach to instability indicated by the $p - \rho$ curve for $\lambda = 7$ (Fig. 6(a)) seems to reflect this situation.) A happier degree of compatibility exists between the

third mode shape and the early bending deformations around $\lambda = 10$, and in this region the third mode scallop of the modified shell and the $p_{cr} - \lambda$ curve of the clamped shell are similar. Analogous situations recur as λ increases, but already at $\lambda = 13$ the initial bending boundary layer (Fig. 10(a)) is so small that only small deviations of p_{cr} from 1 are found.

Not unexpectedly, the curves of Fig. 7 corresponding to initially imperfect shells follow the same trend as that for the perfect shell. (For a smaller range of λ similar results -- not directly comparable, however, because of different choices of imperfection shape -- were calculated by Chen in Ref. 6 by the energy method.) The reductions in p_{cr} caused by downward imperfections of amplitudes 2 1/2 $^{o}/o$ and 5 $^{o}/o$ of the shell rise are substantial, but, except near $\lambda = 4$, not enough to produce even fair agreement with the experimental data shown in Fig. 7. Furthermore, imperfections of negative sign -- upward with respect to the perfect shell -- actually increase p_{cr} at $\lambda = 4$ and 6.

Kaplan and Fung measured the initial contours of their test specimens; reduction of their measured imperfections to the presently considered form (57) reveals that they had values of ε that averaged about .15. But it seems evident from the present theoretical results that consideration of even such large imperfections would still not fully close the gap between experiment and axisymmetric buckling theory for $\lambda \geq 6$.

The implication seems inescapable that a rational explanation of the experimental results must incorporate consideration of non-axisymmetric initial imperfections and deformations. The modified shell has a spectrum of eigenvalues associated with buckling modes having nodal diameters as well

as circles; for λ greater than about 6, the clamped shell would probably choose to amplify similar initial imperfections and buckle in a non-axisymmetric pattern. In contrast to the situation for axisymmetric imperfections, the influence of an imperfection that is antisymmetric through the center is obviously independent of sign. It can only be speculated now that the quantitative influence on p_{cr} of an unsymmetrical imperfection would be greater than that of an axisymmetric one of comparable magnitude, but this seems essential if the experimental results are to be explained. Finally, there is experimental evidence favoring unsymmetrical buckling for $\lambda > 6$. Most of the shells tested by Homewood, Brine and Johnson snapped into a configuration with the maximum buckle depth off center, as did about half of the specimens of Kaplan and Fung in the range $\lambda > 6$. Furthermore, even a final buckled shape that is axisymmetric might be reached through a succession of unsymmetrical states, as has been shown clearly by high speed photographs taken by Kloppel and Jungbluth (Ref. 14) of the buckling process of some non-shallow spherical shells.

APPENDIX A

Calculations of Kernel Functions G and H

Note that $G(x,\xi)$ as given by Eq. (35) may be written

$$G(x,\xi) = \frac{\partial}{\partial x}\left[\int_0^\infty \left(\frac{a^2}{a^4+1}\right)J_0(ax)J_1(a\xi)da\right] \qquad (A1)$$

Next, consider the Bessel function of the second kind $Y_1(z)$ in the complex plane; if the negative imaginary axis is taken as a branch line, then for x real and positive

$$Y_1(-x) = -Y_1(x) - 2iJ_1(x)$$

(See, for example, Ref. 15.) Then, the integral in the brackets of Eq. (A1) is given by

$$I = -\frac{1}{2i}\int_0^\infty \left(\frac{a^2}{a^4+1}\right)J_0(ax)\left[Y_1(a\xi) + Y_1(-a\xi)\right]da$$

$$= -\frac{1}{2i}\int_{-\infty}^\infty \left(\frac{a^2}{a^4+1}\right)J_0(ax)Y_1(a\xi)da \qquad (A2)$$

where the Cauchy principal value of the integral is understood.[1] The integral may also be written

$$I = \frac{1}{2}\int_{-\infty}^\infty \left(\frac{a^2}{a^4+1}\right)J_0(ax)H_1^{(1)}(a\xi)da$$

wherein the Hankel function of the first kind

$$H_1^{(1)} = J_1 + iY_1$$

has been introduced.

---

[1] This trick has been described by Sneddon (Ref. 11, p. 476); the writer is indebted to Professor G. F. Carrier for suggesting its use.

The asymptotic behavior of the integrand (see Ref. 15) is such that for $0 \leq x \leq \xi$, contour integration in the upper half-plane is feasible for the evaluation of I, and the result, by residue theory, is

$$I = \frac{\pi}{4}\left[i^{\frac{1}{2}}J_0(xi^{\frac{1}{2}})H_1^{(1)}(\xi i^{\frac{1}{2}}) + i^{-\frac{1}{2}}J_0(xi^{3/2})H_1^{(1)}(\xi i^{3/2})\right] \qquad (0 \leq x \leq \xi) \tag{A3}$$

In terms of the Kelvin functions, defined by

$$\text{ber } x + i \text{ bei } x = J_0(xi^{3/2})$$

$$\text{ker } x + i \text{ kei } x = K_0(xi^{1/2})$$

where K_0 is the modified Bessel function defined by $K_0(x) = -\frac{\pi}{2} H_0^{(1)}(ix)$ the result (A3) can be reduced to

$$I = \text{bei } x \text{ ker}'\xi + \text{ber } x \text{ kei}'\xi \qquad (0 \leq x \leq \xi)$$

The final result (37) then follows by differentiation, and the symmetry of G.

The kernel H is given by

$$H(x,\xi) = \frac{\partial L}{\partial x}$$

where

$$L = \int_0^\infty \left(\frac{1}{\alpha^4+1}\right)J_0(\alpha x)J_1(\alpha\xi)d\alpha$$

$$= \int_{-\infty}^{\infty} \left(\frac{1}{\alpha^4+1}\right)J_0(\alpha x)H_1^{(1)}(\alpha\xi)d\alpha$$

Then

$$L = \text{ber } x \text{ ker}'\xi - \text{bei } x \text{ kei}'\xi + \frac{1}{\xi}$$

(this time there is a non-zero contribution from the semi-residue at the origin) and the result (38) for H follows.

APPENDIX B

The Basic Solutions A_1 , B_1 , A_2 , and B_2

The solutions of (39) and (40) satisfying the boundary conditions (41) and (42) are

$$\begin{cases} A_1(x) = \frac{1}{D}(\text{ber}'\lambda\ \text{bei}'x - \text{bei}'\lambda\ \text{ber}'x) \\ B_1(x) = -\frac{1}{D}(\text{ber}'\lambda\ \text{ber}'x + \text{bei}'\lambda\ \text{bei}'x) \end{cases}$$

where

$$D = (1+\nu)\left[(\text{ber}'\lambda)^2 + (\text{bei}'\lambda)^2\right] - \lambda(\text{ber}\ \lambda\ \text{bei}'\lambda - \text{bei}\ \lambda\ \text{ber}'\lambda)$$

The solutions satisfying the boundary conditions (43) and (44) are

$$A_2(x) = -(1+\nu)B_1(x) - \frac{\lambda}{D}(\text{ber}\ \lambda\ \text{bei}'x - \text{bei}\ \lambda\ \text{ber}'x)$$

$$B_2(x) = (1+\nu)A_1(x) + \frac{\lambda}{D}(\text{ber}\ \lambda\ \text{ber}'x + \text{bei}\ \lambda\ \text{bei}'x)$$

The constants ρ_1 and ρ_2 (Eqs. (56), (57)) are easily found from the differential equation (40); thus

$$x^2B'' + xB' - B = x^2A$$

and so, by integration

$$\int_0^\lambda x^2A\,dx = \lambda^2B'(\lambda) - \lambda\,B(\lambda)$$

Thus

$$\rho_1 = B_1'(\lambda) - \frac{1}{\lambda}B_1(\lambda)$$

and similarly for ρ_2 . Use of (42) then gives

$$\rho_1 = \frac{1}{\lambda}\left[1 - (1-\nu)\,B_1(\lambda)\right]$$

and similarly (44) leads to

$$\rho_2 = -\frac{1}{\lambda}(1-\nu)B_2(\lambda)$$

APPENDIX C

Analysis of Shell with Modified Boundary Conditions

For the perfect, shallow spherical shell supported as shown by the upper sketch in Fig. 8, the membrane state $\theta = 0$ and $\bar{\phi} = -2px$ is truly an exact solution. The buckling pressure parameter $\bar{p}$ for this modified shell is found by setting

$$\bar{\phi} = -2\bar{p}x + \phi \tag{C1}$$

in Eqs. (19) and (20), and dropping non-linear terms in ϕ and θ. The resulting linear equations are

$$(x\theta')' - \frac{\theta}{x} + x\phi = -2\bar{p}x\theta \tag{C2}$$

$$(x\phi')' - \frac{\phi}{x} - x\theta = 0 \tag{C3}$$

The boundary conditions are $\theta = 0$ and $\phi = 0$ at $x = \lambda$, the latter condition following from the equilibrium requirement $\bar{\phi}(\lambda) = -2\bar{p}\lambda$.

The spectrum of solutions to this eigenvalue problem is

$$\theta_n = J_1\left(\frac{r_n x}{\lambda}\right) \tag{C4}$$

$$\phi_n = -\left(\frac{\lambda}{r_n}\right)^2 J_1\left(\frac{r_n x}{\lambda}\right) \tag{C5}$$

where

$$J_1(r_n) = 0 \qquad (n = 1, 2, 3, \ldots.) \tag{C6}$$

and the corresponding critical pressures are

$$\bar{p}_n = \frac{1}{2}\left[\left(\frac{\lambda}{r_n}\right)^2 + \left(\frac{r_n}{\lambda}\right)^2\right] \quad (n = 1, 2, 3, \ldots.) \tag{C7}$$

The roots r_n of (C5), obtained from Ref. 16, are given in Table 2, below; the scalloped curve in Fig. 8 shows the variation of the lowest

critical pressure with λ. The mode shapes (C4) corresponding to $n = 1, 2, 3, 4$ are plotted in Fig. 10(b).

The post-buckling behavior of the modified shell may be determined approximately by means of a simple Galerkin solution. Substituting

$$p = \bar{p}_n + f \tag{C8}$$

$$\theta = AJ_1\left(\frac{r_n x}{\lambda}\right) \tag{C9}$$

$$\Phi = -2px - B\left(\frac{\lambda}{r_n}\right)^2 J_1\left(\frac{r_n x}{\lambda}\right) \tag{C10}$$

into (19) and (20), multiplying these equations by $J_1\left(\frac{r_n x}{\lambda}\right)$, and integrating from zero to λ, gives

$$\left(\frac{\lambda}{r_n}\right)^2 (A-B) + 2Af_n + \frac{AB\lambda d_n}{r_n^2} = 0 \tag{C11}$$

$$B - A + \frac{A^2}{2\lambda} d_n = 0 \tag{C12}$$

where

$$d_n = \frac{2\int_0^1 \left[J_1(r_n\xi)\right]^3 d\xi}{\lambda\left[J_0(r_n)\right]^2} \tag{C13}$$

The constant d_n is identical with Archer's constant C_n^{nn} calculated numerically by him in Ref. 3, with the results as shown in Table 2.

Elimination of B from (C11) and (C12) gives

$$f = \frac{1}{4}\left(\frac{\lambda}{r_n}\right)^2 \left[-3\alpha + \alpha^2\right] \tag{C14}$$

where

$$a = \left(\frac{d_n}{\lambda}\right)A$$

The average deflection is given by

$$\bar{w} = \bar{w}_1 + \bar{w}_2$$

where

$$\bar{w}_1 = \left[\frac{4(1-\nu^2)H}{\lambda^2}\right] \bar{p}_n \qquad (C15)$$

is the average deflection due to the pure contraction of the shell before buckling, and $\bar{w}_2$ is the post-buckling contribution to $\bar{w}$. Then (see Eq. 52)

$$\bar{w}_2 = \left[\bar{w}_2\right]_{r=a} + \frac{2H}{\lambda^4}\int_0^\lambda x^2\theta\, dx \qquad (C16)$$

But note that the modified boundary conditions require that

$$\left[\bar{w}_2\right]_{r=a} = -\frac{a}{2H}\left[u_2\right]_{r=a}$$

where u_2 is the horizontal displacement during buckling, and, by (5),

$$\left[u_2\right]_{r=a} = \frac{a}{Et}\left[\frac{d\psi_2}{dr} - \nu\frac{\psi_2}{r}\right]_{r=a}$$

where ψ_2 is the post-buckling change in the stress function ψ. Then

$$\bar{w}_2(\lambda) = -\frac{\lambda t^2}{24H(1-\nu^2)}\left[\lambda\bar{\phi}_2'(\lambda) - \nu\bar{\phi}_2(\lambda)\right] \qquad (C17)$$

where $\bar{\phi}_2 = \bar{\phi}(x) + 2\bar{p}_n x$ is the change in $\bar{\phi}$ after buckling. Then, the non-dimensional average-deflection parameter ρ (Eq. 54) becomes, from (C15), (C16), and (C17)

$$\rho = 2(1-\nu)\bar{p}_n - \left[\Phi_2'(\lambda) - \frac{\nu}{\lambda}\Phi_2(\lambda)\right] + \frac{1}{\lambda^2}\int_0^\lambda x^2\theta\, dx$$

But since $\theta(x)$ and $\Phi_2(x)$ should satisfy Eq. (20), a manipulation similar to that preceding Eq. (51) of the text may be applied, giving

$$\Phi_2'(\lambda) = \frac{1}{\lambda}\Phi_2(\lambda) + \frac{1}{\lambda^2}\int_0^\lambda x^2\theta\, dx - \frac{1}{2\lambda^2}\int_0^\lambda x\theta^2\, dx$$

Vertical equilibrium now imposes the condition $\Phi(\lambda) = -2p\lambda$; hence $\Phi_2(\lambda) = -2\lambda(p-\bar{p}_n)$, and so

$$\rho = 2(1-\nu)p + \frac{1}{2\lambda^2}\int_0^\lambda x\theta^2\, dx \qquad (C18)$$

Substituting (C4) into the integral in (C18) gives

$$\rho = 2(1-\nu)p + \frac{1}{4}\left[J_0(r_n)\right]^2 A^2$$

or (C19)

$$\rho = 2(1-\nu)p + \frac{\lambda^2}{dn^2}\left[J_0(r_n)\right]^2 a^2$$

The information in Eqs. (C8), (C14), and (C19) can now be summarized as follows:

(a) Before buckling

$$\begin{aligned} &(p < \bar{p}_n\ ,\ a = 0) \\ &p = 2(1-\nu)\rho \end{aligned} \qquad (C20)$$

(b) After buckling

$$\begin{cases} p = \bar{p}_n + \frac{1}{4}\left(\frac{\lambda}{r_n}\right)^2(-3a+a^2) \\ \rho = 2(1-\nu)p + \frac{1}{4}\left(\frac{\lambda}{r_n}\right)^2 b_n\, a^2 \end{cases} \qquad (C21)$$

where

$$b_n = \frac{r_n^2}{d_n^2}\left[J_0(r_n)\right]^2$$

The constants b_n are tabulated in Table 2.

The post-buckling variation of p with ρ is given parametrically by Eqs. (C21). Typical $p - \rho$ curves (with $\nu = \frac{1}{3}$) are given in Fig. 9 for several λ's, for $\alpha \geq 0$. Note that $\alpha < 0$ would give quite different curves, involving no reduction in p; hence it may be presumed that $\alpha \geq 0$ -- meaning <u>downward</u> buckling at the center -- is always preferred.

REFERENCES

1. V. I. Feodosiev, "Calculation of Thin Clicking Membranes" (in Russian), Prikladnaia Matematika i Mekhanika, Vol. X, p. 295, 1946.

2. A. Kaplan and Y. C. Fung, "A Nonlinear Theory of the Bending and Buckling of Thin Elastic Shallow Spherical Shells", NACA Technical Note 3212, August 1954.

3. R. R. Archer, "Stability Limits for a Clamped Spherical Shell Segment under Uniform Pressure", Quarterly of Applied Mathematics, Vol. XV, p. 355, January 1958.

4. E. L. Reiss, H. J. Greenberg and H. B. Keller, "Nonlinear Deflections of Shallow Spherical Shells", Journal of the Aeronautical Sciences, Vol. 54, p. 533, July 1957.

5. H. J. Weinitschke, "On the Nonlinear Theory of Shallow Spherical Shells", Journal of the Society for Industrial and Applied Mathematics, Vol. 6, p. 209, September 1958.

6. W. L. Chen, "Effect of Geometrical Imperfection on the Elastic Buckling of Shallow Spherical Shells", Sc.D. Thesis, Department of Civil and Sanitary Engineering, Massachusetts Institute of Technology, January 1959.

7. G. P. R. von Willich, "The Elastic Stability of Thin Spherical Shells", Journal of the Engineering Mechanics Division, Proceedings of the American Society of Civil Engineers, Vol. 185, No. EM 1, January 1959. See also Discussion by W. L. Chen, Vol. 85, No. EM 2, April 1959.

8. H. S. Tsien, "A Theory for the Buckling of Thin Shells", Journal of the Aeronautical Sciences, Vol. 9, p. 373, August 1942.

9. E. Reissner, "Symmetric Bending of Shallow Shells of Revolutions", Journal of Mathematics and Mechanics, Vol. 7, p. 121, March 1958.

10. K. Marguerre, "Zur Theorie der gekrümmten Platte grosser Formanderung", Proceedings of the Fifth International Congress of Applied Mechanics, p. 93, 1938.

11. I. N. Sneddon, "Fourier Transforms", McGraw-Hill, New York, 1951.

12. E. Reissner, "Stresses and Small Displacements of Shallow Spherical Shells, II", Journal of Mathematics and Physics, Vol. 25, p. 279, January 1947.

13. R. H. Homewood, A. C. Brine and A. E. Johnson, Jr., "Buckling Instability of Monocoque Shells", paper presented at meeting of the Society for Experimental Stress Analysis, May 1959, Washington, D. C. (to be published in SESA Proceedings).

14. K. von Kloppel and O. Jungbluth, "Bettrag zum Durchschlag Problem dunnwandiger Kugelschalen", Der Stahlbau, Vol. 22, p. 121, 1953.

15. N. W. McLachlan, "Bessel Functions for Engineers", Oxford University Press, London, 1934.

16. E. Jahnke and F. Emde, "Tables of Functions", Dover Publications, New York, 1945.

TABLE 1

BUCKLING PRESSURES

(a) Perfect Shell			(b) Imperfect Shell			
λ	p_{cr}	Prescribed Parameter	λ	ε	p_{cr}	Prescribed Parameter
3.5	.614	ρ	4	-.025	.617	ρ
4	.578	ρ	4	-.050	.659	ρ
5	.629	ρ	4	.025	1.061	ρ
5.5	.789-.79	ρ,p	4	.050	1.116	ρ
6	.995	ρ	6	.025	.90-.91	p
7	1.068	ρ	6	.050	.62-.63	p
8	1.130	ρ	8	.025	1.03-1.04	p
9	.931-.94	ρ,p	8	.050	.93-.94	p
10	.822-.83	ρ,p	10	.025	.78-.79	p
11	.83-.84	p	12	.025	.83-.84	p
12	.96-.97	p	12	.050	.75-.76	p
13	.96-.97	p				

TABLE 2

CONSTANTS IN ANALYSIS OF MODIFIED SHELL

n	r_n	d_n	b_n
1	3.83	1.012	2.33
2	7.02	.818	6.62
3	10.17	.901	7.95
4	13.32	.846	11.82
5	16.47	.883	13.44

Note: For large n, $d_n \rightarrow \sqrt{3}/2$, $b_n \rightarrow (8/3\pi)r_n$

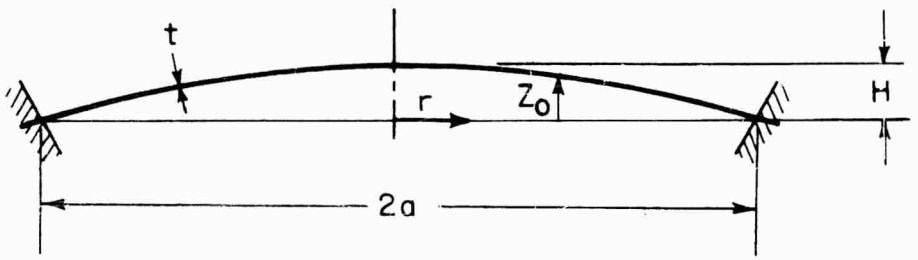

FIG. 1 CLAMPED SHALLOW SHELL OF REVOLUTION

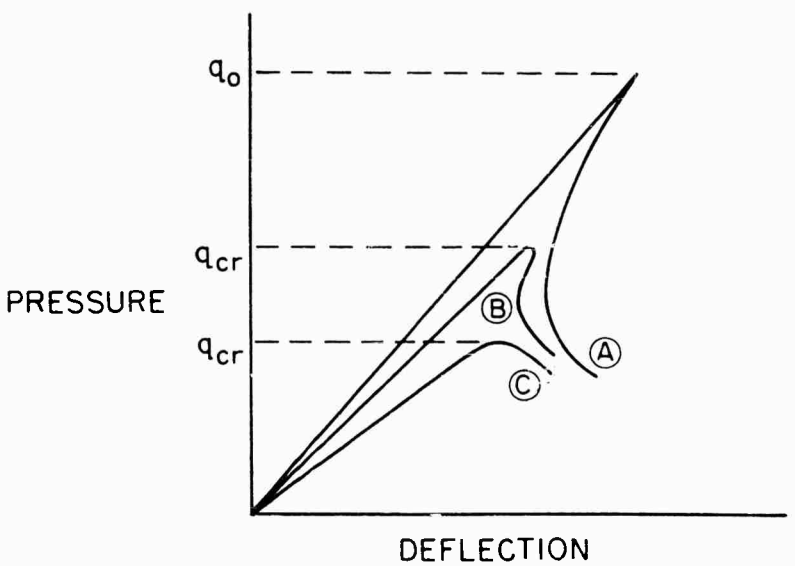

FIG. 2 PRESSURE-DEFLECTION CURVES FOR PERFECT (A) AND IMPERFECT (B) (C) COMPLETE SPHERICAL SHELLS

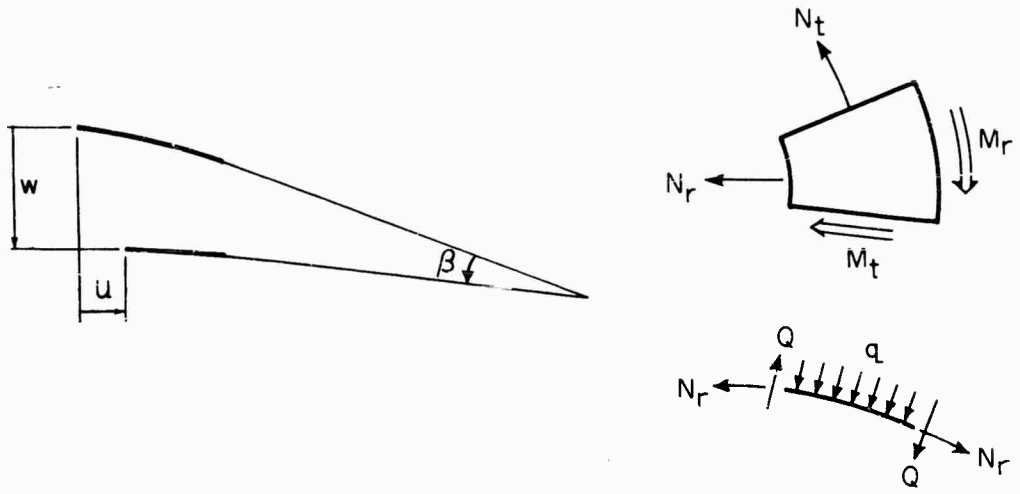

FIG. 3 DISPLACEMENTS, ROTATION, FORCES AND MOMENTS

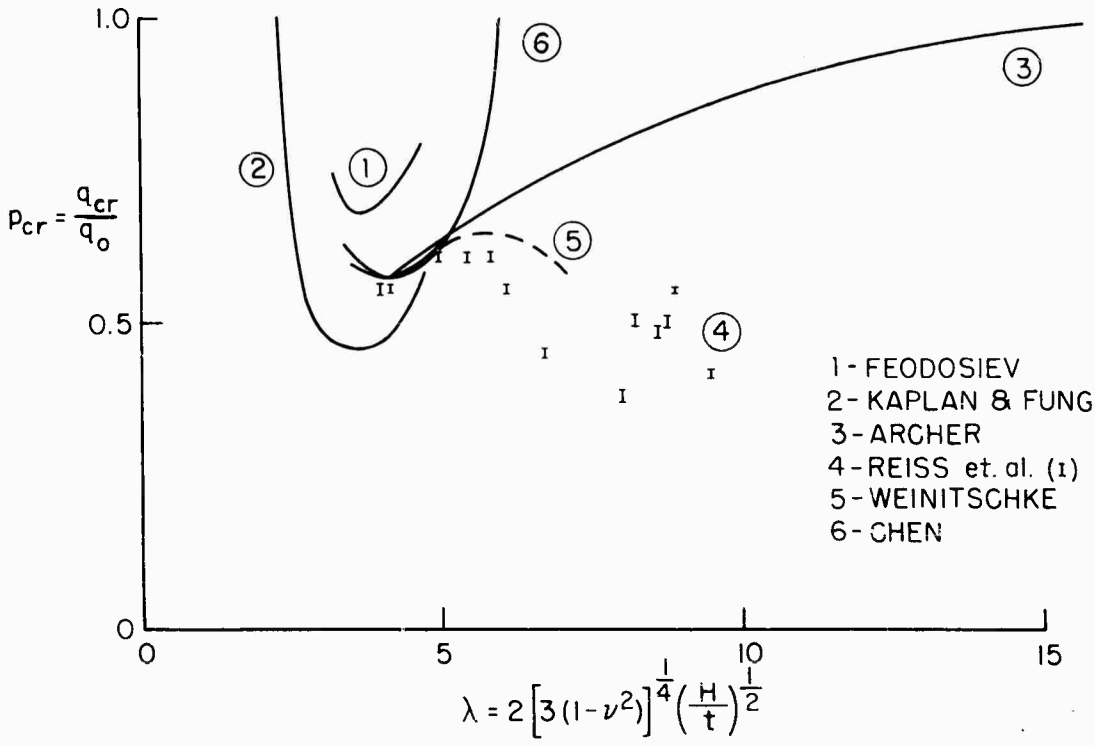

FIG. 4 PREVIOUS RESULTS FOR BUCKLING PRESSURES OF CLAMPED SHALLOW SPHERICAL SHELLS

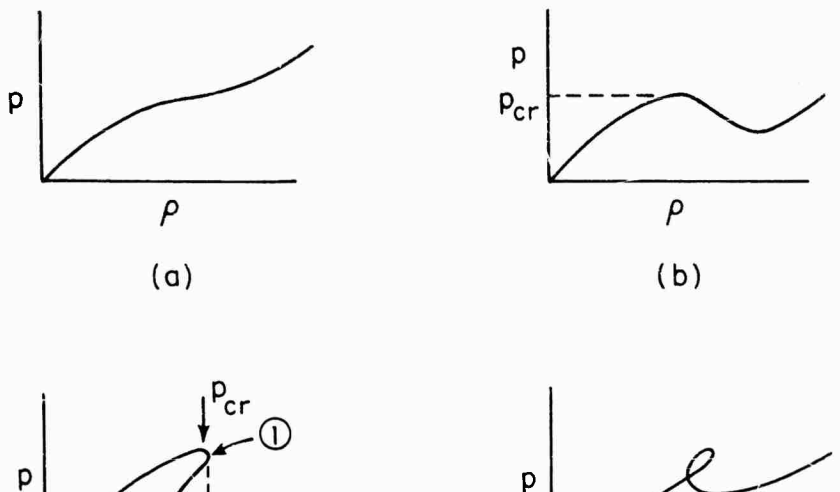

FIG. 5 HYPOTHETICAL CURVES OF PRESSURE VS. AVERAGE DEFLECTION

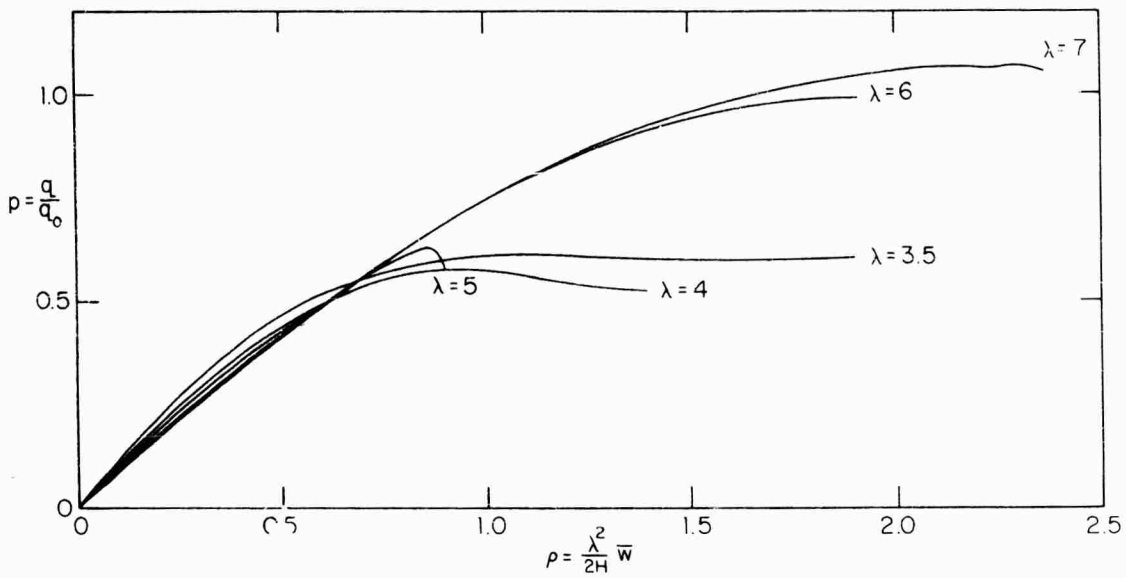

(a)

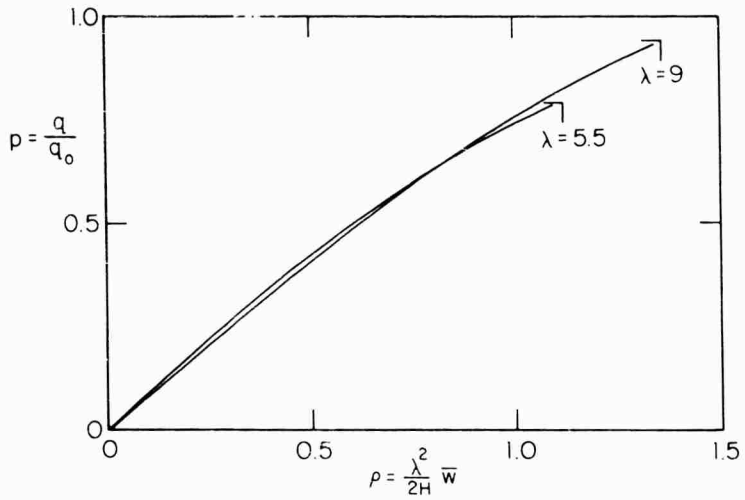

(b)

FIG. 6 PRESSURE VERSUS AVERAGE DEFLECTION OF CLAMPED SHALLOW SPHERICAL SHELLS

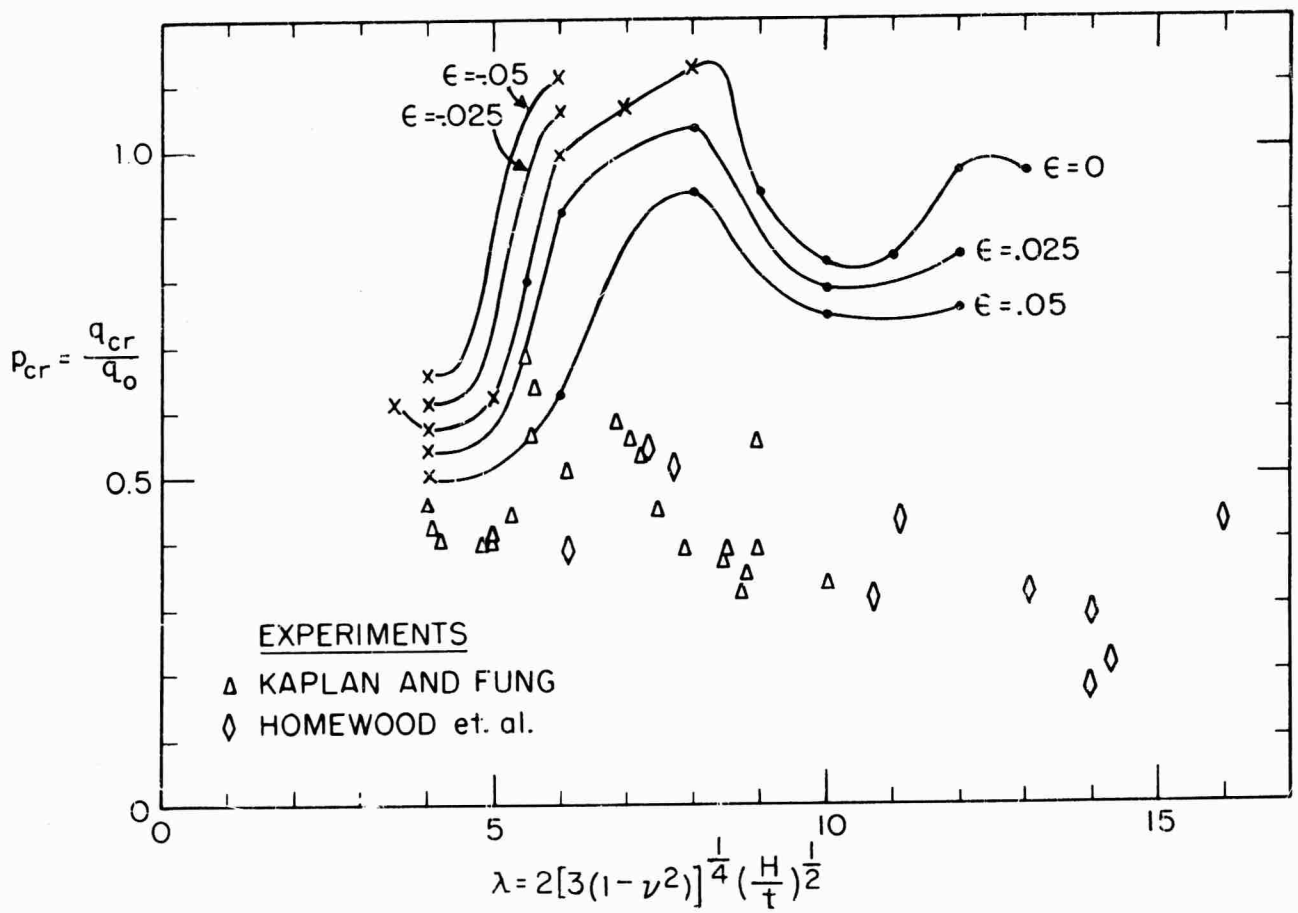

FIG. 7 CALCULATED BUCKLING PRESSURES OF INITIALLY PERFECT AND IMPERFECT CLAMPED SHALLOW SPHERICAL SHELLS AND EXPERIMENTAL RESULTS

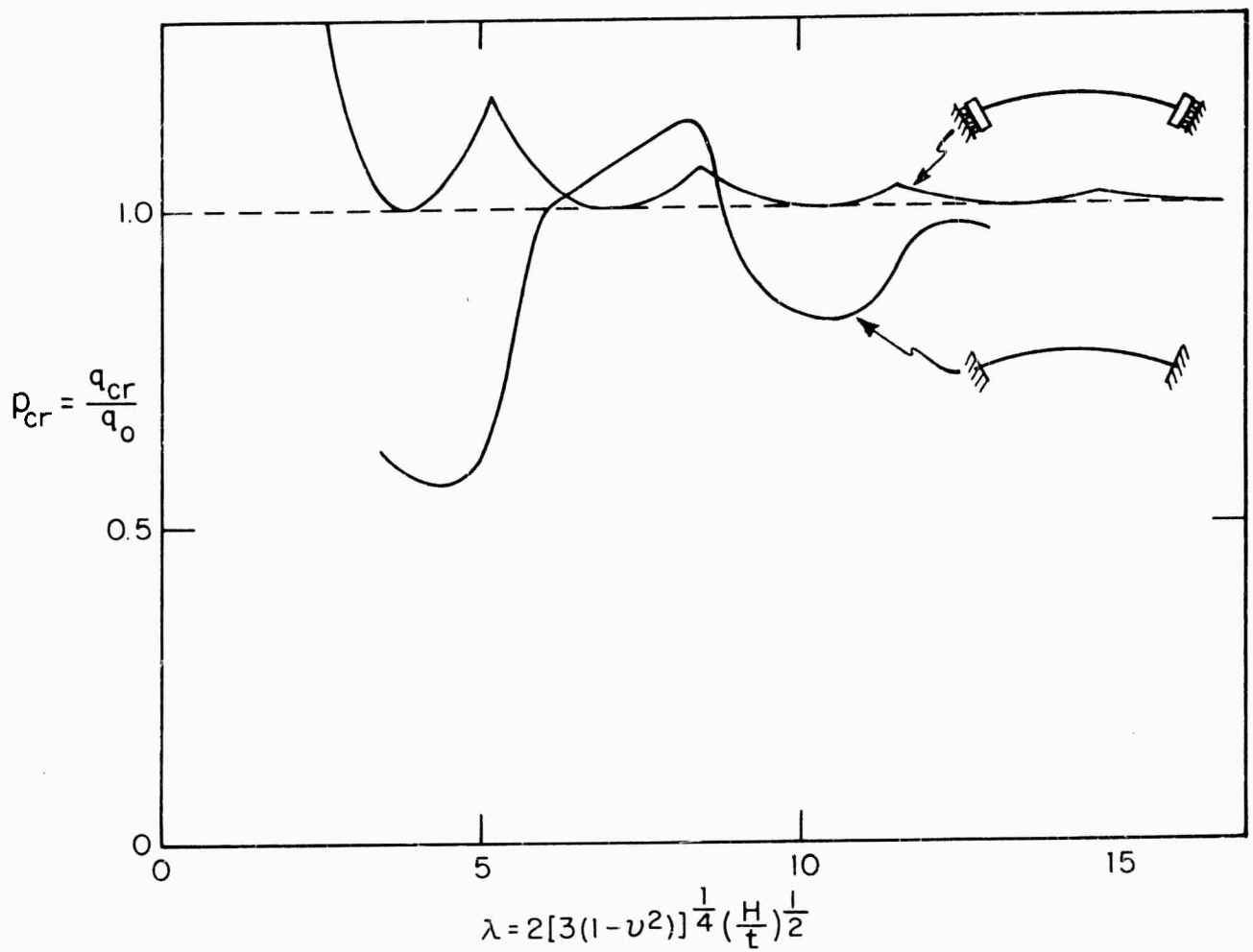

FIG. 8 COMPARISON OF AXISYMMETRIC BUCKLING PRESSURES OF CLAMPED SHALLOW SPHERICAL SHELL AND OF MODIFIED SHELL

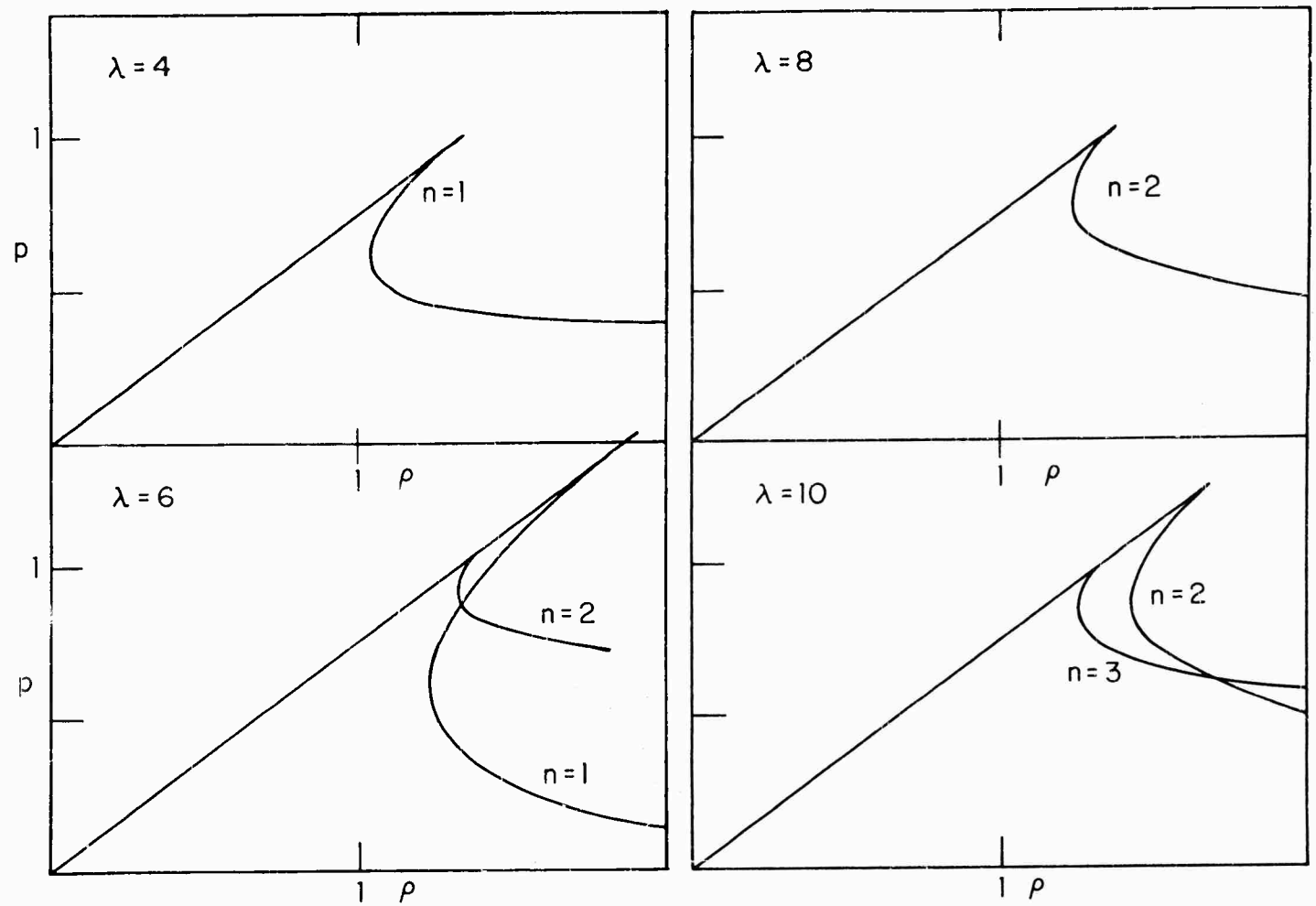

FIG. 9 VARIATION OF PRESSURE WITH AVERAGE DEFLECTION OF THE MODIFIED SHELL

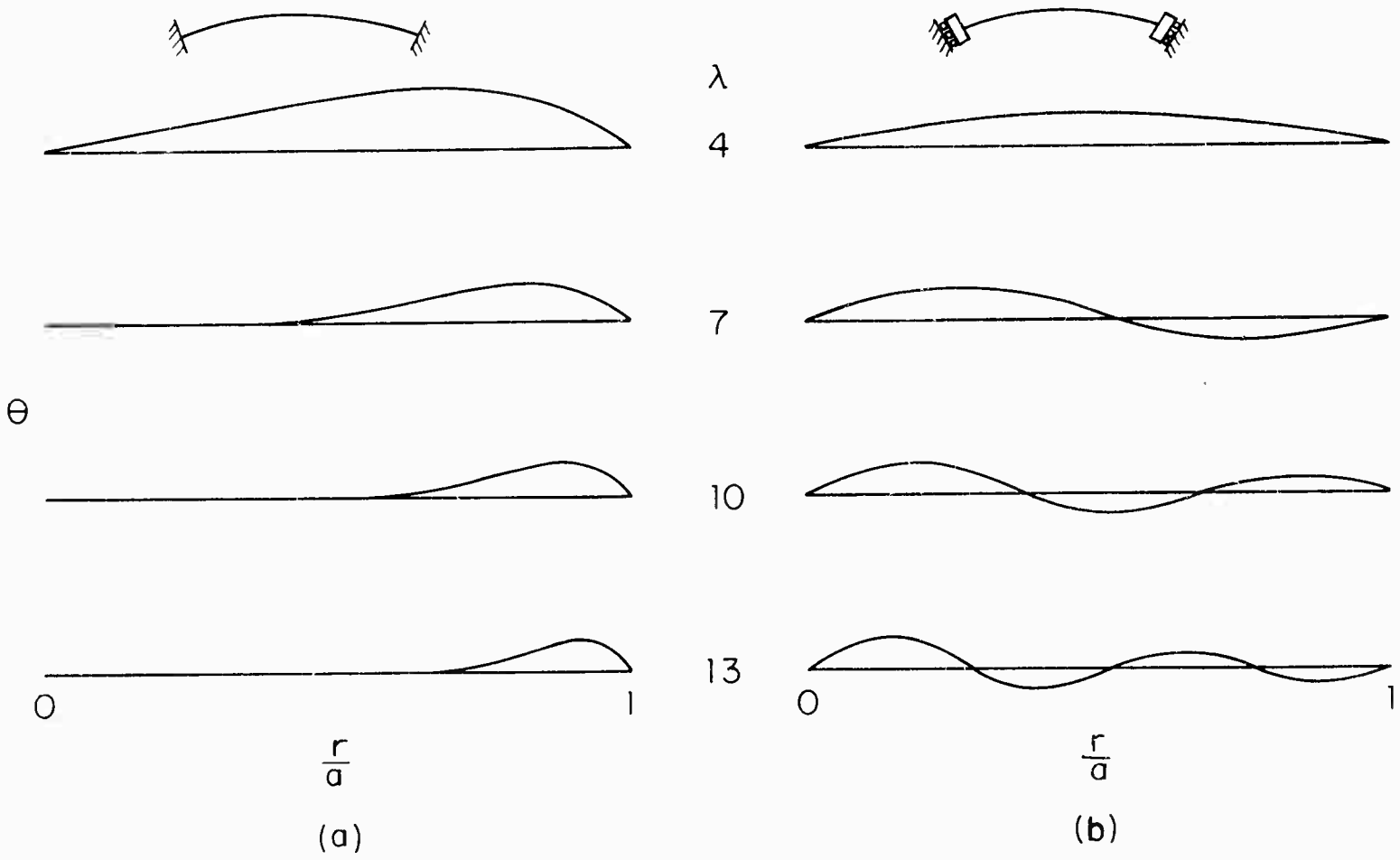

FIG. 10 COMPARISON OF (a) EARLY (LINEAR THEORY) ROTATIONS OF CLAMPED SHELL AND (b) BUCKLING ROTATIONS OF MODIFIED SHELL

Harvard U.

ERRATA

OFFICE OF NAVAL RESEARCH

Contract Nonr 1866(02)

Technical Report No. 5

August 1959

BUCKLING OF CLAMPED SHALLOW SPHERICAL SHELLS

by

Bernard Budiansky

	Incorrect	Corrected
Eq. (10)	$-qr^2$	$-\frac{1}{2}qr^2$
Eq. (19)	$-2px$	$-2px^2$
Eq. (26)	$-2px$	$-2px^2$
Eq. (32)	$y^*(\alpha) \int_0^\infty xJ_1(\alpha x)y(x)dx$	$y^*(\alpha) = \int_0^\infty xJ_1(\alpha x)y(x)dx$
Eqs. (35), (36)	$d\xi$	$d\alpha$